Journal of Sound and Vibration (1998) **214**(5), 885–901
Article No. sv981578

DAMPING BEHAVIOUR OF SHAPE MEMORY ALLOYS: STRAIN AMPLITUDE, FREQUENCY AND TEMPERATURE EFFECTS

M. C. Piedboeuf and R. Gauvin

Centre de recherche appliquée sur les polymères, Ecole Polytechnique de Montréal, CP 6079, *Succ*. "*Centre-ville*", *Montréal, Québec H3C 3A7, Canada*

and

M. Thomas

Ecole de Technologie Supérieure, 1100 *rue Notre-Dame, Montréal, Québec, H3C* 1*K*3, *Canada*

(*Received* 9 *May* 1997, *and in final form* 17 *February* 1998)

An extensive study of the effects of frequency and strain amplitude as well as temperature on the damping behaviour of superelastic NiTi shape memory alloy wires was undertaken. A full factorial design taking into account the two-level interactions between these variables has been conducted. The dissipated energy and the loss factor were analyzed. Analysis shows that an increase in temperature has no effect on the dissipated energy while it decreases slightly the loss factor. Both however increase with the increase in strain amplitude. A maximum in dissipated energy and in the loss factor is observed around 0·1 Hz. Both factors then decrease as the frequency continues to increase. This behaviour is also strain amplitude dependent. A thermal analysis showed that the observed frequency and frequency–amplitude interaction effects are due to an important temperature variation produced by the energy generated during the transformation. Finally, a three harmonic Fourier sine series model is proposed to model the shape memory alloy dynamic behaviour. Frequency, amplitude and temperature effects are taken into account and dissipated energy and the loss factor can be determined from this model.

1. INTRODUCTION

With the present increasing emphasis on environmental control, the problem of containing severe vibration and noise in mechanical devices, either operating at high speed or during impact loading, receives considerable attention. This is why materials which are able to reduce vibration and noise are becoming more and more technologically important. The desired properties of high strength, stiffness and tolerance to adverse environments seemed to be incompatible with high internal damping for most materials. Highly viscoelastic materials do show high damping capacities but often have insufficient strength. Recently, some high damping metals have been developed which combine high inherent damping with relatively high strength properties. One of the processes that lead to high energy dissipation in metals is phase transformation, and in particular martensitic transformation which occurs in Shape Memory Alloys (SMA) [1].

Shape memory alloys are two-phase alloys with the austenite being the high temperature phase and the martensite being the low temperature phase. Phase transformation in these alloys can either be temperature induced or stress induced. This leads to shape change.

0022–460X/98/300885 + 17 $30.00/0

Atoms and defects move and reorientation of martensite results in large energy dissipation. In these materials, the two phases can coexist over a certain temperature range, and three main contributions to the damping are considered. They are the damping due to the thermally induced transformation, the damping related to the stress induced transformation, and finally, the intrinsic damping generated in the two coexisting phases [2]. Dissipation coming from temperature variation occurs during heating or cooling. Over the past few decades, extensive research efforts have been devoted to understand this mechanism [2–4]. However, not many practical applications are found for the damping generated by thermally induced transformation.

From a practical point of view, the two other energy dissipation mechanisms offer a more interesting perspective. The intrinsic damping of the martensitic phase is quite high due to the reorientation of the martensite twin variants under stress. Some applications of martensitic alloys as dampers have been considered [1, 5, 6]. In the austenitic phase, the intrinsic damping is low but if the applied stress is high enough, martensite can be stress induced and this phase transformation will lead to high energy dissipation. Figure 1 shows the stress–strain curve of an austenitic shape memory alloy. When the stress reaches the transformation level σ_{Ms}, martensite will be induced and this transformation will continue until all the austenite has been transformed at an almost constant stress level. Upon release of the stress, the martensite unloads elastically down to a stress level σ_{As}, where it will transform back to austenite, once again at an almost constant stress level. Once this transformation is completed, there is a final elastic unloading of the austenite phase. This is known as the superelastic effect since there is no permanent deformation even if the behaviour is non-linear. The surface hysteresis which is equal to the volumetric energy dissipated in a cycle during this transformation is quite high and gives rise to the interesting damping capacities of these alloys. If the martensite is stress induced at a higher temperature, the transformation stresses will increase linearly and shift the curve upward as shown by the dashed lines in Figure 1. Applications of superelastic SMA to increase damping have also been considered [1, 5, 6] with special interest in aseismic isolation [7] or passive structural damping of beams [8]. SMA are much stronger than most viscoelastic materials and relatively insensitive to environmental hazard. One of the advantages of using them in the austenitic or superelastic state is that they can provide a restoring force

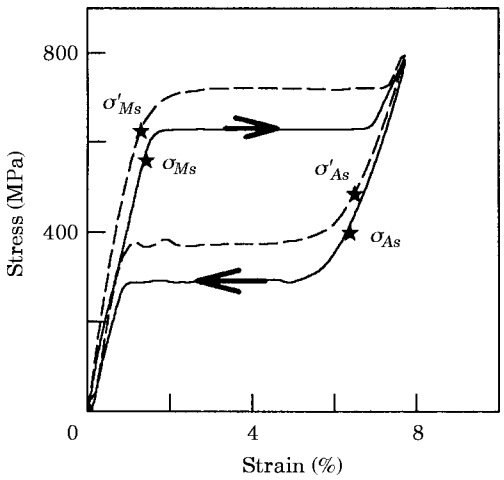

Figure 1. Superelastic stress–strain curve of a shape memory alloy. σ_{Ms} and σ_{As} are the stresses to start the martensitic and the reverse austenitic transformation respectively. The dashed curve is for a solicitation at a higher temperature.

which helps restore the overall structure to its original position after any imposed deformation. The usefulness of such materials will be governed by the temperature–frequency–vibration amplitude ranges in which the damping capacity is sufficiently elevated, and by the stability of damping under operating conditions.

Yet not much has been done to study the superelastic damping capacities of SMA. Dejonghe *et al*. [4] performed a series of tests to study the mechanisms of energy dissipation in Copper SMA. Among them, tensile tests where martensite was stress induced in an austenitic alloy allowed the calculation of the dissipated energy ΔW from the surface of the energy hysteresis, and of an internal friction factor defined as $\delta = \frac{1}{2}(\Delta W/W)$, where W is the strain energy. This factor decreased exponentially with the temperature due to the fact that strain energy increases with temperature because there is an increase in transformation stresses with temperature. Tobushi *et al*. [6] performed tensile tests on superelastic NiTi SMA and studied the dissipated energy as a function of strain amplitude and temperature. They showed that dissipated energy increases linearly with an increase in strain amplitude since there is more martensite formed in the alloy. They also observed a slight increase of this energy with the SMA temperature but no explanation of this phenomenon was given.

An interesting study was done by Van Humbeeck and Delaey [9]. Tensile tests at different uniform strain rates varying from 0·000033 s^{-1} to 0·067 s^{-1} were done on copper SMA. A maximum of the dissipated energy and the internal friction at an intermediate strain rate was observed. Temperature measurement of the samples showed that this effect could be due to the variation of temperature resulting from the exo, endothermic martensitic transformation. It was also concluded that the energy dissipated is temperature independent.

Actually, little research has been done on NiTi alloys and even less under dynamic conditions. This study is related to an ongoing research project on the use of SMA reinforcement to add passive damping to polymer matrix composites. For this purpose, austenitic NiTi wires 100 μm in diameter, were chosen. The first part of this project was to study the superelastic behaviour of the wires in tensile testing. First under uniform strain rate [10] and then, as presented in this paper, under sinusoidal loading to study their damping capacity. In this study, tests were performed at three levels of vibration amplitude (2, 3 and 4% of strain), over four decades of frequency (0·01, 0·1, 1, 5 and 10 Hz) and at two temperature levels (25 and 35 °C). All possible combination of these variables were tested. The results are statistically analyzed and a thermal analysis is done to determine the temperature effect contribution to the results. Finally, a simple model for the dynamic behaviour of the SMA using Fourier series is proposed and used to evaluate the dissipated energy and the loss factor.

2. EXPERIMENTAL PROCEDURE

2.1. SAMPLES

The NiTi wires, with a diameter of 100 μm, are straight annealed and chrome doped (0·2%) for a better superelastic effect. Their transition temperatures were determined by testing them in tension, at a strain rate of 0·0017 s^{-1} (10 mm/min) for different temperatures. These transition temperatures were found to be $-25°C$ for the austenitic start (As) and $-81°C$ for the martensitic start (Ms). To get a good grip on the wires for the tensile tests, they were glued on cardboard tabs [10]. Prior to testing, so as to stabilize the superelastic effect, each wire had to be precycled for 100 cycles at 5 Hz and 4·5 % cyclic deformation. Figure 2 shows the stress–strain curves obtained at the beginning and after

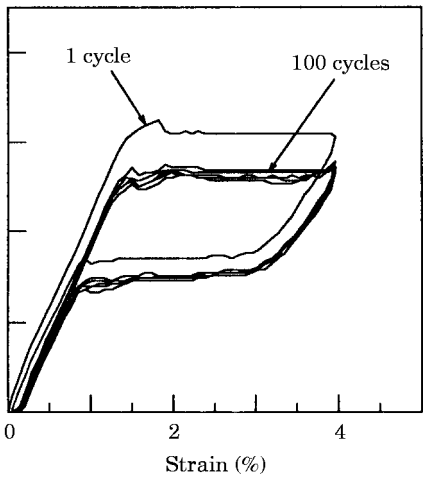

Figure 2. Curves obtained after 1, 50, 100, 125, 150 and 200 cycles at 4·5% of precycling deformation.

50, 100 and up to 200 cycles, which clearly demonstrate the stabilisation effect after 100 cycles.

2.2. EQUIPMENT

Tests were made on a servo hydraulic machine equipped with a 50 N load cell. Data acquisition was made at a sampling rate of 1000 samples/s on each test. The deformation was measured as the overall displacement of the cross head; the difference between this measurement and the actual wire extension is negligible due to the stiffness of the loading frame and the small loads and large deformations present in the wire. Tests were run in a controlled temperature chamber.

2.3. EXPERIMENTAL DESIGN AND TESTING PROCEDURE

The samples were loaded under a cyclic, tensile, sinusoidal deformation $\epsilon = \epsilon_0(1 - \cos(\omega t))$ in a deformation controlled mode. A full factorial design was selected so that all interactions between the independent variables could be effectively investigated. The independent variables in this study were: the frequency of excitation, the maximum peak to peak strain amplitude and the temperature of the chamber. The levels of these independent variables are shown in Table 1. 4% was chosen as the maximum peak to peak vibration amplitude since it is roughly the maximum deformation a glass fiber can withstand in a composite. Four samples were tested for each set of testing parameters, for

TABLE 1

Levels of independent variables used in the tests

		Level				
Variable	Unit	1	2	3	4	5
Frequency f	Hz	0·01	0·1	1	5	10
Maximum amplitude $2\epsilon_0$	%	2	3	4	–	–
Temperature $T°$	°C	25	35	–	–	–

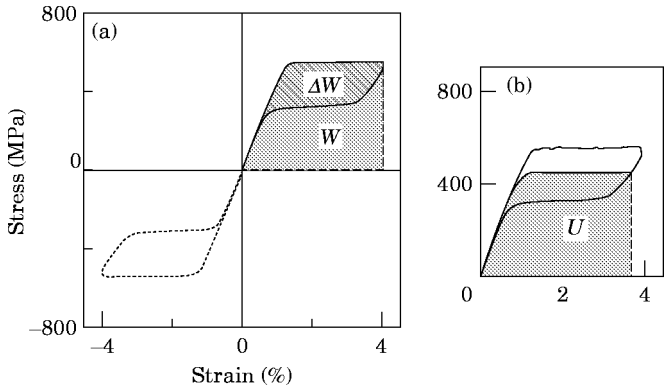

Figure 3. (a) Superelastic curve in tension (——) and in compression (– – –). ΔW and W are respectively the dissipated energy and the maximum strain energy in a tensile loading–unloading solicitation. (b) U is the maximum potential energy in a tension–compression solicitation.

a total of 60 samples tested. All these samples were tested first at 25°C and then at 35°C, thus resulting in a total of 120 experiments. The parameters studied (dependent variables) were the dissipated energy by cycle ΔW (J/m^3/cycle) which is the area of the energy hysteresis, and the loss factor defined as $\eta = (1/2\pi)(2\Delta W/U)$ where U is the maximum potential energy [11]. These parameters are shown in Figure 3. Loss factors are usually defined for a full cyclic deformation in tension compression. If such a deformation is applied on a SMA, the stress–strain curve in compression can be considered similar to the one in tension as shown by the dotted lines in Figure 3. In cyclic loading, the total dissipated energy is then equal to twice the energy dissipated in tension. This is the reason for the factor 2 associated with the dissipated energy ΔW in the loss factor equation presented earlier. For linear viscoelastic material with low damping, the maximum potential energy U is equal to $\frac{1}{2}\epsilon_{max}\sigma_{max}$, but for a non-linear material a more precise definition is $U = W - \frac{1}{2}\Delta W$ [12], where W is the maximum strain energy at ϵ_{max} as shown in Figure 3 and $\frac{1}{2}\Delta W$ is the energy dissipated up to this point. These values were determined by numerical integration.

Analysis of variance (ANOVA) was applied to investigate the main effects of the independent variables (ϵ_{max}, f, T°) together with their interaction effects on dependent variables.

3. RESULTS

3.1. TESTS RESULTS

Since Anova analysis revealed that there was no significant variation between the samples, the graphical results presented here are for one typical sample and not average values. To illustrate the interaction effect of temperature and maximum amplitude, the stress–strain curves obtained for the various amplitudes and temperatures at a frequency of 0·1 Hz are shown in Figure 4. As was said earlier, an increase in temperature causes a linear increase in transformation stresses and a shift of the stress–strain curves upward as can be seen on this figure. This will increase the maximum strain energy but there is no evident effect of temperature on the dissipated energy. The increase in amplitude causes an increase of the dissipated energy as well as an increase in maximum strain energy W, as could be expected.

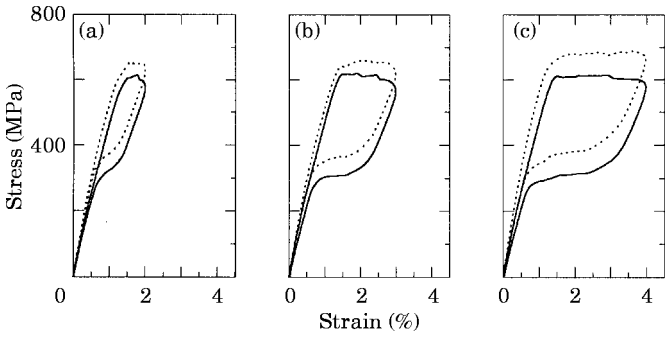

Figure 4. Stress–strain curves at a frequency of 0·1 Hz at (a) 2% amplitude, (b) 3% amplitude, (c) 4% amplitude, and 25°C (——) and 35°C (· · · ·).

Figure 5 illustrates the effect of frequency by showing the results of samples tested at 25°C and 4% of amplitude at four different frequencies. As can be observed, up to 0·1 Hz, the stress difference between the two plateaus increases, producing an increase in the surface hysteresis, and also in the dissipated energy; For higher frequencies, the lower plateau deforms and rises, causing a pronounced reduction of the surface hysteresis. This may be due to a variation of the samples temperature and will be discussed later in this article.

3.2. STATISTICAL ANALYSIS

ANOVA analysis is an effective method of analyzing complex and numerous results when interactions between the independent variables may arise. Essentially, this analysis determines whether the discrepancies between the average results at the different levels of a parameter are greater than could reasonably be expected from the variation that occurs within the results at a specific level of the parameter. The analysis of variance table is a valuable device due to Box *et al*. [13], which allows for the evaluation of the hypothesis that there is no difference between the results at the different levels of the parameters. The ANOVA output and the calculated F ratio for a confidence interval of 95% are shown in Tables 2 and 3 for the dissipated energy and the loss factors. The F-ratios compare the mean square of an effect (main or interaction) to the residual mean square; if this ratio is close to one, there is no significant difference. p is the probability of accepting this hypothesis as determined from the F probability table; if this probability is lower than 0·05, then there is a significant effect. Interactions are shown only for significant effects

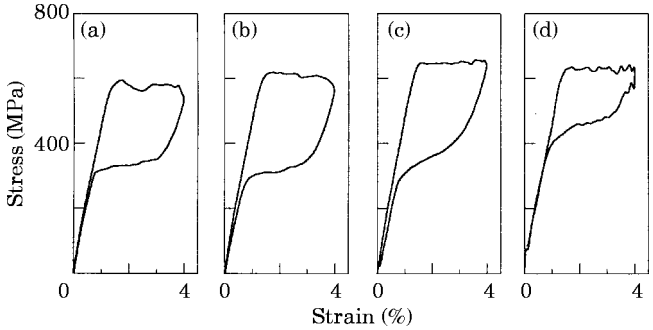

Figure 5. Stress–strain curves at 25°C and 4% of amplitude for four different frequencies: (a) 0·01 Hz; (b) 0·1 Hz; (c) 1 Hz and (d) 10 Hz.

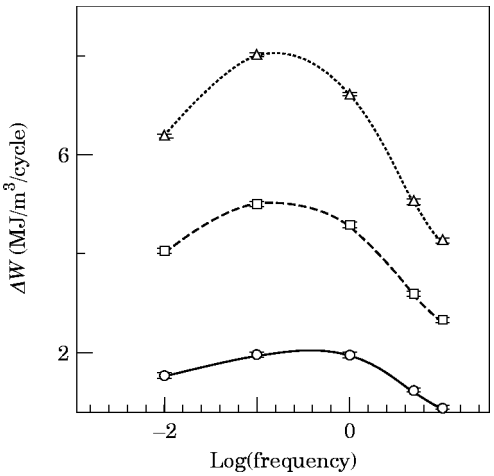

Figure 6. Variation of the average values of the dissipated energy at 2% (——), 3% (- - - -) and 4% (· · · ·) of amplitude.

($p < 0{\cdot}05$). All the observed effects have a statistical probability of more than 99%, which is very significant. Results are plotted in Figures 6 and 7 with their confidence intervals.

3.2.1. *Temperature effect and amplitude and frequency interaction on dissipated energy (ΔW)*

Table 2 shows that the dissipated energy is affected by the three independent variables with some interactions between amplitude and frequency. In fact, analysis of the results shows that the ambiant temperature effect was negligible. As can be seen in Figure 4, when the amplitude increases, so does the dissipated energy. The dissipated energy is proportional to $(\epsilon_{max} - \epsilon_{Ms})$ where $\epsilon_{max} = 2\epsilon_0$ is the peak to peak vibration amplitude and ϵ_{Ms} is the deformation at which the martensite transformation begins. Also, frequency interacts with the amplitude. For instance, at 2% strain, there is only a slight variation in dissipated energy by varying frequency, while at 4% the variation is more important and the maximum occurs at around 0·1 Hz. At higher frequencies, dissipated energy decreases. Moreover, at 2% amplitude the maximum occurs at a slightly higher frequency than for the higher amplitudes. As it was shown in a previous paper [14], there is an

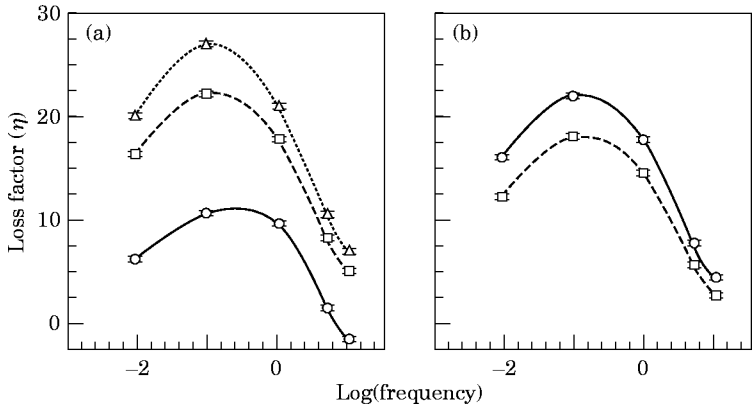

Figure 7. Variation of the average values of the loss factor with (a) the amplitude at 2% (——), 3% (- - - -) and 4% (· · · ·), and with (b) the temperature at 25°C (——) and 35°C (– – –).

TABLE 2

Anova and F ratio for dissipated energy ΔW (d.f.: degree of freedom)

Source of variation	Sum of squares	d.f.	Mean square	F ratio	Sig. level
Main effects					
A: Temperature	6·72e4	1	67 203	25·19	0·0000
B: Deformation	1·1e8	2	54 954 357	20 595·33	0·0000
C: Frequency	2·35e7	4	5 876 700	2202·42	0·0000
Interaction					
BC	4 737 996	8	592 249	221·96	0·0000
Residual	240146	90	2668	–	–
Total (corrected)	1·39e8	119			

important temperature variation of the samples as the strain rate increases. It could be the reason for the behaviour observed here and is studied in more details in section 4 of this paper.

3.2.2. *Temperature effect and amplitude and frequency interaction on the loss factor* (η)

Table 3 shows that the loss factor is affected by the three variables with some interactions between deformation and frequency, and temperature and frequency. As can be seen from the last graph of Figure 7, the difference in behaviour at 25 and 35°C is less important at higher frequency than at the low frequency.

To get a better understanding of the loss factor variations, it helps to look at the maximum potential energy $U = W - \frac{1}{2}\Delta W$ as a function of the different variables. Figure 8 shows the variations of U as a function of temperature and frequency at the different amplitudes. Since the maximum strain energy W increases with ambient temperature in the same way as do the transformation stresses while the dissipated energy ΔW is not much affected by the temperature, the potential energy U increases with temperature which causes a decrease in the loss factor as the ambient temperature increases. The maximum potential energy increases with the frequency, and this increase is more pronounced at higher amplitudes. Since dissipated energy decreases with frequencies higher than 0·1 Hz, the decrease of the loss factor which is proportional to $\Delta W/U$ is more pronounced. The interaction with amplitude is also more pronounced for the loss factor since the increase

TABLE 3

Anova and F ratio for the loss factor η (d.f.: degree of freedom)

Source of variation	Sum of squares	d.f.	Mean square	F ratio	Sig. level
Main effects					
A: Temperature	0·00414	1	0·00414	402·32	0·0000
B: Deformation	0·047368	2	0·02368	2301·55	0·0000
C: Frequency	0·070685	4	0·01767	1717·25	0·0000
Interactions					
AC	4·083e − 4	4	1·02e − 4	9·92	0·0000
BC	2·921e − 3	8	3·65e − 4	35·48	0·0000
Residual	0·000926	90	1·03e − 6	–	–
Total (corrected)	0·126567	119	–	–	–

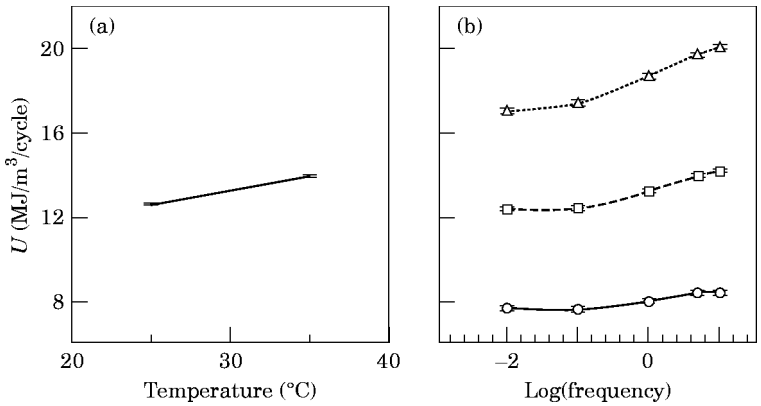

Figure 8. Variation of the average values of the maximum potential energy with (a) the temperature, and (b) the amplitude at 2% (——), 3% (- - - -) and 4% (· · · ·).

of potential energy U is more important at 4% of amplitude than at 2%. These phenomena may be due to a thermal effect and will be investigated in the next section.

4. THERMAL ANALYSIS

4.1. THEORY

It has been mentioned that frequency effects and frequency–amplitude interaction may be a temperature effect due to the nature of the transformation: the austenite–martensite transformation is exothermic and the martensite–austenite transformation is endothermic. The energy generated by this transformation is proportional to the volume fraction of martensite formed and is at its maximum in the middle of the transformation. At a high strain rate, the heat generated by the austenitic–martensitic transformation may not have time to dissipate and this will cause the sample temperature to increase. So, the transformation stress will rise which, in turn, will produce an increase of the slope of the upper plateau in the stress strain curve. During the reverse transformation, the mechanism will be similar with a cooling of the specimen which will not have time to absorb enough heat at high strain rate. The presence of such effects was shown by different authors [9, 15].

The importance of this phenomenon depends on the quantity of heat generated, which is a property of the material, and of the size of the specimen. For large samples, the temperature effect will be predominant with increasing difficulty of energy dissipation, while for small samples it may be minimized to a certain limit. It was shown in a previous paper [14] that even if the wire diameter is very small, important heat effects occur as strain rate increases. Therefore, a simplified thermal analysis was performed to determine the importance of that effect in the case of a sinusoidal loading.

4.2. SIMULATION

The problem is to determine the temperature of a long rod having a large length to diameter ratio, 100 mm over 0·1 mm. Thermal energy is generated in the specimen by transformation and by internal friction. This energy can usually be dissipated by convection, radiation and conduction. Due to the small area of the wire, the dissipation by radiation is negligible as well as radial conduction. For conduction through the gripping fixture, since the samples are very long compared to their diameter and are fixed on cardboard with epoxy glue which make a good thermal insulation, it is assumed to be

negligible as well. So the only significant heat dissipation process considered in this case is the convection process.

With the assumptions that at any time t the temperature of the wire is uniform and that constant properties exist, the conservation of energy law can be applied. For a time interval Δt small enough for the assumptions to be valid, it is expressed in a discreet form as

$$E_g - E_{out} = \Delta E_{st}, \tag{1}$$

where E_g is the energy generated, E_{out} is the energy leaving through the surface and ΔE_{st} is the variation of energy stored within the volume. The energy outflow is due to convection and is given by

$$E_{out} = h(\pi DL)(T - T_\infty), \tag{2a}$$

where h is the convection heat transfer coefficient, D and L are the diameter and the length of the wire respectively, and $(T - T_\infty)$ is the difference between the sample temperature T and the room temperature T_∞. The convection heat transfer coefficient is a function of the temperature difference $(T - T_\infty)$ [16]. This relation can be expressed as

$$h = h_\infty (T - T_\infty)^{1/3}, \tag{2b}$$

with h_∞ and h being the convection coefficients at room temperature and at the sample temperature respectively.

The variation in thermal energy storage is due to the temperature change in the sample,

$$\Delta E_{st} = \rho V c\, \Delta T, \tag{3}$$

where ρ is the density, V the volume of the sample and c the specific heat. ΔT is the sample's temperature change over the time interval Δt.

As said previously, the energy generation is due to two phenomena, $E_{g(tr)}$ and $E_{g(FI)}$, which are the austenitic–martensitic transformation energy and the internal friction energy respectively. The energy generated by the transformation for a time Δt is given by

$$E_{g(tr)} = \rho V\, \Delta H\, \Delta f(\epsilon), \tag{4}$$

where ΔH is the transformation enthalpy and $\Delta f(\epsilon)$ represents the fraction of energy generated during the time interval Δt. It was shown [14] that the best model to represent this energy generation is a linear increase of energy generation during the transition between the elastic deformation of the austenite and the uniform transformation to martensite, followed by a uniform rate of energy generation once the upper plateau is reached in the stress–strain curve, and ending by a linear decrease at the end of the transformation.

The second energy generation term is due to the dissipative process associated with the phase change in the material. It occurs during the transformation and is mainly due to displacements of atoms. It is proportional to the surface of the energy hysteresis of the stress–strain curve HYS (J/m^3). This energy generation term is given by

$$E_{g(FI)} = V\, \Delta HYS, \tag{5}$$

where ΔHYS is the energy generated during the time interval Δt. Half the hysteresis energy is dissipated during loading and the other half during unloading. If this dissipation process is assumed uniform, the rate of viscous energy dissipation by unit of strain, Δhys, can be determined from the tests results. ΔHYS is then given by

$$\Delta HYS = \Delta hys\, \Delta \epsilon, \tag{6}$$

where $\Delta\epsilon$ is the increment of strain during the time interval Δt. It is given by

$$\Delta\epsilon = \epsilon(t + \Delta t) - \epsilon(t), \tag{7}$$

where $\epsilon = 2\epsilon_0(1 - \cos(\omega t))$.

By using equations (2)–(7) in conjunction with equation (1), the increment in temperature for a time interval Δt can be determined. The sample temperature can be determined for each strain level during the cyclic deformation by incrementing the strain by $\Delta\epsilon$ and computing the new temperature reached for each increment.

All the values used for this computation are given in Table 4. The coefficients $h_\infty c$, and ΔH were taken from references [17–19]. In the present case, the convection heat transfer coefficient was increased since a fan was used in the controlled temperature chamber to insure a uniform air temperature distribution. For the specific heat coefficient c, the same value was used for the austenite and the martensite phase, so an average value of the martensitic and austenitic coefficients was taken. The other values in the table were obtained from the test results. To simplify the problem, these values were supposed to be independent of strain rate and ambient temperature, and the following assumptions were made: (1) ϵ_{Ms}, ϵ_{As} and ϵ_{Af} are the same for all cases; (2) for ΔHYS the average value of the tests made at 4% of deformation, 25°C and a uniform strain rate of 0·0017 s^{-1} was taken; Δhys was determined from this value and assumed constant for all cases.

Since the values of the strain to begin and end the transformations are not very much affected by the test conditions, the first assumption can be justified. As for the second assumption, the value of the hysteresis is strongly dependent on strain rate as can be seen in Figure 7. But since this energy generation term is an order of magnitude smaller than the energy generated by the transformation, its influence is not important and a constant value can be assumed.

4.3. RESULTS

Figure 9 shows the sample temperature versus the deformation for each frequency at 2% and 4% of maximum amplitude and 25°C. The behaviour is the same at 25 and 35°C, the sample temperature being 10° higher at 35°C, so only the results at 25°C are presented. At 0·01 Hz, an equilibrium is established between the energy generation and the energy outflow so that the sample quickly reaches a stable temperature. The increase in temperature at this point is not very important (2°C at 4%).

TABLE 4

Values of the coefficients used in the thermal simulation

Property	Symbol, source	Value
Diameter (m)	D	1×10^{-4}
Length (m)	L	0·1
Density (kg/m^3)	ρ	6500
Convection (W/m^2°C)	h_∞	32·5
Specific heat (J/kg°C)	c	750
Transformation enthalpy (kJ/kg)	ΔH	25
Internal friction (kJ/m^3)	ΔHYS	2600
Martensitic start (%)	ϵ_{Ms}	1
Austenitic start (%)	ϵ_{As}	$2\epsilon_0$† − 0·5
Austenitic end (%)	ϵ_{Af}	0·5
Time increment (s)	Δt	1/500f

†$2\epsilon_0$ = maximum amplitude

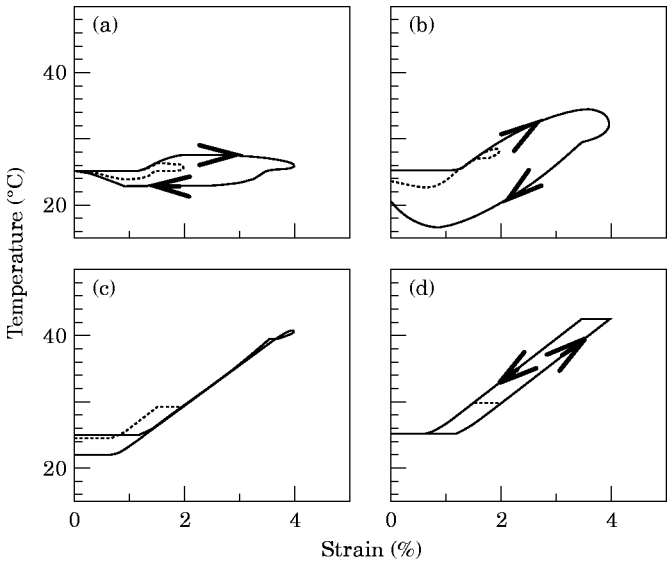

Figure 9. Sample temperature as a function of strain at four levels of frequency: (a) 0·01 Hz, (b) 0·1 Hz, (c) 1 Hz and (d) 10 Hz, and two amplitudes: 2% (· · · ·) and 4% (——), as determined by the simulations.

As the frequency increases and the cycling period decreases, the energy does not have enough time to dissipate, and the sample temperature increases steadily. At 0·1 Hz, the increase in temperature during loading will produce an increase of the upper plateau stress. During unloading, the sample temperature gets lower than the room temperature which will result in a decrease of the lower plateau stress. So there is an increase in the stress hysteresis that results in higher energy dissipation as observed. With ensuing increase in frequency, the temperature during unloading will stay higher than room temperature and produce an increase in the lower plateau stress. This is the reason for the decrease in hysteresis and dissipated energy that was observed. When the frequency reaches 1 Hz and continues to increase up to 10 Hz, the temperature variation during loading remains the same which explains the stability of the maximum strain energy as seen in Figure 8.

At 2% of maximum amplitude, the general behaviour as a function of the frequency is similar to the one at 4% of maximum amplitude, but the maximum temperature reached is not as important (30°C versus 42°C). With less martensite produced, there is less energy generated and not as much temperature variation. This is the reason for the amplitude–frequency interaction and the difference in behaviour at amplitudes of 2 and 4% observed in Figure 6. So the thermal simulation shows that frequency effects and frequency–amplitude interaction are mainly temperature effects due to the energy generated during the transformation.

5. DYNAMIC MODELLING

5.1. THEORY

Modelling the shape memory alloys behaviour under dynamic loading is not a simple task due to the complex stress–strain–temperature relations and the numerous factors that affect this behaviour. Some models use constitutive equations based on thermomechanical relations [20, 21], others use models based on experimental results [22]. But all these models can be applied in simple cases only and at low uniform strain rate. In the literature, no attempt to model dynamic behaviour of shape memory alloys was found.

Since SMA have a highly non-linear viscoelastic behaviour, under a sinusoidal strain variation the stress response is non-simusoidal. This prevents the utilisation of the parameter normally used in linear viscoelasticity such as the elastic modulus E' for the part of the response which is in phase with the sollicitation, the loss modulus E'' for the other part of the response and the loss factor defined as $tg\delta$ where δ is the phase angle between the response and the solicitation.

When non-linearity arises, different theories have been proposed [23, 24], such as the multiple integrals theory [25]. They are often used with polymers since non-linearity usually occurs even at low strain for these materials. But these theories can be applied in isothermal situations and with "simple materials" only (no yield points as an example). It was shown in the previous section that SMA behaviour is non-isothermal, so even the usual non-linear viscoelastic theories cannot be used. However, it can be observed that under sinusoidal loading all these non-linear theories lead to a response in the form of a series of sines and cosines. This follows Fourier's theory saying that any periodic functions may be represented as a series of sines and cosines terms. So to model the behaviour of any kind of materials, a Fourier series of the form

$$Y = Y_0/2 + \sum_{i=1}^{n} Y_{iR} \cos(i\omega t) + \sum_{i=1}^{n} Y_{iI} \sin(i\omega t), \tag{8}$$

where the R indices are for the real part of the response, in phase with the loading, and I is for the imaginary part, out of phase with the loading, can then be used. Since all the coefficients are functions of the dependent variables, this form of equation is interesting if the series can be limited to a restricted number n of harmonics.

5.2. FAST FOURIER TRANSFORM MODEL FOR SMA

The identification of the SMA dynamic behaviour using the Fourier series has been found sufficiently accurate by using three harmonics in the Fourier series development. From the experimental stress results, the sine series coefficients have been calculated using a Fast Fourier Transform (FFT). It was observed that Y_0 and Y_{1R} were important, while Y_{1I}, Y_{2R} and Y_{2I} were an order of magnitude lower and the Y_3 coefficients were two orders of magnitude lower. The other terms were much smaller and therefore negligible. Figure 10 shows the stress results by comparing a test made at 4% of amplitude and 25°C with

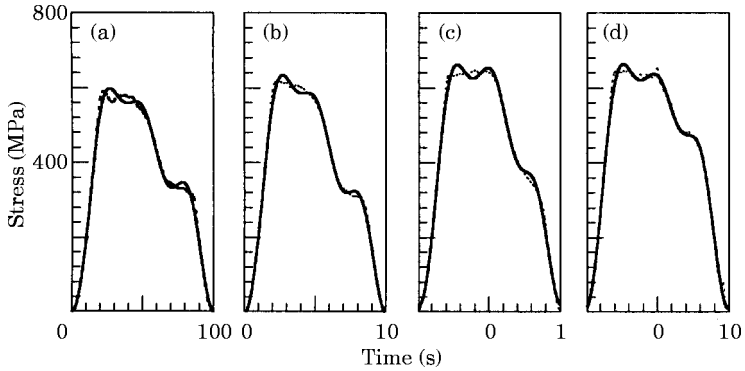

Figure 10. Fourier three harmonic sine series simulation of the stress–time experimental results at 25°C and 4% of strain amplitude at four different frequencies: (a) 0·01 Hz, (b) 0·1 Hz, (c) 1 Hz and (d) 10 Hz. The Fourier coefficients are determined from experimental results. Experimental (· · · ·), FFT model (——).

their three harmonics series development. As can be seen, the agreement between the two curves is very good. A very simple model is then obtained where the coefficients can be easily determined from experimental results.

So, for a loading of the form given by

$$\epsilon = 2\epsilon_0(1 - \cos(\omega t)), \tag{9}$$

the NiTi shape memory alloy has a stress response given by

$$\sigma = \sigma_0 + \sigma_{1R}\cos(\omega t) + \sigma_{1I}\sin(\omega t) + \sigma_{2R}\cos(2\omega t) + \sigma_{2I}\sin(2\omega t) + \sigma_{3R}\cos(3\omega t) + \sigma_{3I}\sin(3\omega t). \tag{10}$$

The model includes seven coefficients which are functions of amplitude, frequency and temperature and for which equations need to be determined. The coefficients were determined for all the tests made in this work. Empirical equations for these coefficients can then be found and are given with their coefficients of determination, R^2, by

$$\begin{aligned}
\sigma_0 &= 232 + 4T + 22\epsilon_0 + 1186\sin(\log(f)) \qquad (R^2 = 92\%),\\
\sigma_{1R} &= -250 - 1{\cdot}8T + 24\epsilon_0 - 54f^{0{\cdot}25} + 4{\cdot}8f \qquad (R^2 = 91\%),\\
\sigma_{1I} &= 52 - 96f^{0{\cdot}27} + 204f^{0{\cdot}1} - 206\epsilon_0^{-1} \qquad (R^2 = 90\%),\\
\sigma_{2R} &= 396 - 1{\cdot}34T - 384\epsilon_0^{0{\cdot}1} - 4{\cdot}6\epsilon_0^{0{\cdot}8}f^{0{\cdot}5} - 2{\cdot}8f^{0{\cdot}4} \qquad (R^2 = 92\%),\\
\sigma_{2I} &= -48 + 0{\cdot}2T + 5{\cdot}2\epsilon_0 f^{0{\cdot}2} \qquad (R^2 = 74\%),\\
\sigma_{3R} &= 60 - 0{\cdot}7T - 26\epsilon_0 + 0{\cdot}6\log(f) \qquad (R^2 = 97\%),\\
\sigma_{3I} &= 8 + 370\epsilon_0^{-4} - 123f^{0{\cdot}15} + 72e_0 f^{0{\cdot}25} \qquad (R^2 = 75\%).
\end{aligned} \tag{11}$$

R^2 is a measure of the precision of an equation to model the data. The constant σ_0 in equation (10) arises from the constant in the deformation. The first harmonic terms may be seen as the linear response of the material associated to the deformation imposed to the material. The other harmonics would then represent the non-linear part of the response. The non linear response can be associated with other forms of deformations such as atomic motion and transformation which may occur at a different frequency than the loading.

5.3. DETERMINATION OF ΔW AND η FROM THE FFT MODEL

From the FFT model, one should be able to determine the dissipated energy and the loss factor. In a stress-strain relation, the energy is given by the equation

$$E = \int \sigma \, \mathrm{d}\varepsilon. \tag{12}$$

From the equations for stress and strain given by the relations (9) and (10), the equation for the energy with the FFT model can be determined and is given by

$$\begin{aligned}
E = \epsilon_0(&-\sigma_0\cos(\omega t) - \tfrac{1}{4}\sigma_{1R}\cos(2\omega t) + \tfrac{1}{2}\sigma_{1I}[t - \tfrac{1}{2}\sin(2\omega t)]\\
&+ \tfrac{1}{2}\sigma_{2R}[\cos(\omega t) - \tfrac{1}{3}\cos(3\omega t)] + \tfrac{1}{2}\sigma_{2I}[\sin(\omega t) - \tfrac{1}{3}\sin(3\omega t)]\\
&+ \tfrac{1}{2}\sigma_{3R}[\tfrac{1}{2}\cos(2\omega t) - \tfrac{1}{4}\cos(4\omega t)] + \tfrac{1}{2}\sigma_{3I}[\tfrac{1}{2}\sin(2\omega t) - \tfrac{1}{4}\sin(4\omega t)].
\end{aligned} \tag{13}$$

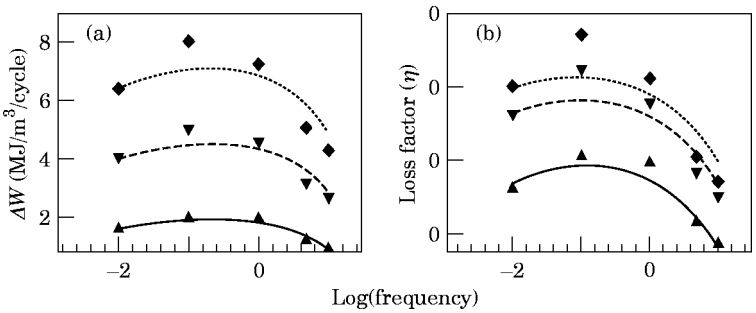

Figure 11. (a) Dissipated energy and (b) loss factor as determined from the FFT model (——), 2%; (- - - -), 3%; (· · · ·), 4% for the SMA dynamic behaviour. Experimental results: ▲ 2%, ▼ 3% and ◆ 4%.

The dissipated energy is the energy evaluated over a complete cycle. Due to the orthogonal properties of sines functions, most of the terms vanish and the relation for ΔW is given by

$$\Delta W = \pi \sigma_{1I} \epsilon_0. \tag{14}$$

This is exactly the same equation that is obtained for a linear viscoelastic material. It means that the dissipated energy is due to the first imaginary harmonic only and a loss modulus $E_1'' = \sigma_{1I}/\epsilon_0$ can be defined for this non-linear viscoelastic material.

The maximum strain energy in the present situation is equation (13) evaluated between 0 and π/ω. So the relation for W is given by

$$W = 2\sigma_0 \epsilon_0 + \tfrac{1}{2}\pi \sigma_{1I} \epsilon_0 - \tfrac{2}{3}\sigma_{2R} \epsilon_0 \tag{15}$$

and since the loss factor in this case is given by $\eta = 1/\pi(\Delta W/U)$, where $U = (W - \frac{1}{2}\Delta W)$, the final equation is

$$\eta = \sigma_{1I}/2(\sigma_0 - \tfrac{1}{3}\sigma_{2R}). \tag{16}$$

So, using equations (14) and (16) including the relations of equations (11) for the coefficients, the dissipated energy and the loss factor can be determined for the Fourier model. Figure 11 shows the results from this model versus the experimental results. The agreement is good at low amplitude but as the amplitudes increase, there is more divergence between the model and the experimental results, specially for the loss factor. There are two main sources of error in the determination of ΔW and η. First, the increasing difficulty to get a perfect sinusoidal deformation as the frequency and amplitude increase, and secondly the error introduced by the truncated Fourier model and by the utilisation of the coefficients from equations (11) for which the coefficients of determination vary from 74–97%. Even if it is not perfectly accurate, the sine series model is very efficient and very useful mainly because the coefficients are easily determined and because it is not mathematically complex.

6. CONCLUSIONS

An extensive study of the effects of frequency, strain amplitude, temperature and their interactions on dissipated energy and loss factor was done on a NiTi shape memory alloy. It was found that ambient temperature has no significant effect on dissipated energy, but the loss factor decreases with an increase in temperature as the transformation stresses, and so the potential energy, increases with the temperature. An increase in strain amplitude produces both an increase in dissipated energy and the loss factor. Concerning the

frequency, a maximum in dissipated energy and in the loss factor was observed around 0·1 Hz. As the frequency continues to increase, there is a pronounced decrease in these two parameters and a sharp decrease of the hysteresis was observed. This behaviour is amplitude dependent, and the variations are more pronounced at 4% than at 2% of strain amplitude.

A theoretical thermal analysis was performed to predict the temperature variation in the samples due to the energy generated by the phase transformation. It was shown that as the frequency increases from 0·01 Hz to 0·1 Hz the shape memory alloy temperature increases in loading and decreases during unloading. This produces an increase in stress hysteresis and so of the dissipated energy and of the loss factor. For higher frequencies, the temperature during unloading increases over the ambient temperature, causing a decrease in dissipated energy. Since there is more transformation, and so more energy generated with the increase in amplitude, these effects are more pronounced at high amplitude. So it can be concluded that the frequency effects and the frequency-amplitude interaction effects are mainly due to a thermal effect.

Finally, a Fourier three harmonic sine series was successfully used to model the dynamic behaviour of the shape memory alloy as a function of frequency, amplitude and temperature. The coefficients were determined by FFT of the experimental results and empirical models for these coefficients were derived. This results in a model very easy to derive and to use. The relations for the dissipated energy and the loss factor determined from this model are very simple.

ACKNOWLEDGMENTS

This work is financially supported by the Natural Science and Engineering Research Council (NSERC) of Canada and the Québec government program FCAR (Formation de Chercheurs et Aide à la Recherche).

REFERENCES

1. D. E. Hodgson 1993 *Proceedings of Damping* '93 *San Francisco*, *BAA*-1. Energy absorption due to cyclic deformation of shape memory alloys.
2. R. De Batist 1992 *MD*: *Mechanics and Mechanisms of Material Damping ASTM STP* **1169**, 45–49. Mechanical energy dissipation related with martensitic transformation processes.
3. H. C. Lin, S. K. Wu and M. T. Yeh 1993 *Metalurgical Transactions A* **24A**, 2189–2194. Damping characteristics of TiNi shape memory alloys.
4. W. Dejonghe, L. Delaey, R. De Batist and J. Van Humbeeck 1977 *Metal Science*, 532–530. Temperature and amplitude dependence of internal friction in Cu–Zn–Al alloys.
5. D. E. Hodgson and R. C. Krumme 1994 *Proceedings of the First International Conference on Shape Memory and Superelastic Technologies*, *California*, *U.S.A.*, 371–376. Damping in structural applications.
6. H. Tobushi, P. H. Lin, K. Tanaka, M. Makita and A. Ikai 1994 *Proceedings of the First International Conference on Shape Memory and Superelastic Technologies*, *California*, 389–394. Deformation behavior of NiTi superelastic alloy subjected to strain variations.
7. P. R. Witting and F. A. Cozzarelli 1993 *Proceedings of Damping* '93 *San Francisco*, *ECC*-1. Design and seismic testing of shape memory structual dampers.
8. P. Thomson, G. J. Balas and P. H. Leo 1995 *Smart Materials and Structures* **4**, 36–43. The use of shape memory alloys for passive structural damping.
9. J. Van Humbeeck and L. Delaey 1981 *Journal de physique* **42**, C5-1007. The influence of strain-rate, amplitude and temperature on the hysteresis of pseudoelastic Cu–Zn–Al single crystal.
10. M. C. Piedboeuf, R. Gauvin and M. Thomas 1997 *Technical report*, *Ecole Polytechnique*, *Montréal*. Superelasticity of NiTi shape memory alloy: strain rate, temperature and strain effects. Part I: experimental results.

11. M. Regelbrugge 1994 *Smart Structures and Materials CLS*^{3}/*ASME*, conference proceedings. Smart structures and materials applications: issues and case studies.
12. E. E. Ungar and E. M. Kerwin, Jr. 1962 *Journal of the Acoustical Society of America* **34**, 954. Loss factors of viscoelastic systems in terms of energy concepts.
13. G. E. P. Box, W. G. Hunter and J. Stuart 1978 *Statistics for experimenters*: *An introduction to design*, *data analysis and model building*. New York: John Wiley.
14. M. C. Piedboeuf, R. Gauvin and M. Thomas 1997 *Technical report*, *Ecole Polytechnique*, *Montréal*. Superelasticity of NiTi shape memory alloy. Part II: thermal analysis.
15. P. H. Leo, T. W. Shield and O. P. Bruno 1993 *Acta Metallurgical Material* **41**, 2477–2485. Transient heat effects on the pseudoelastic behavior of shape-memory wires.
16. F. P. Incropera and D. P. DeWitt 1990 *Fundamentals of Heat and Mass Transfer*. New York: John Wiley.
17. J. P. Holman 1986 *Heat Transfer*. New-York: McGraw-Hill.
18. T. Waran 1992 *Actuators Design Using Shape Memory Alloys*. Canada: T. Waran.
19. E. Patoor and M. Berveiller 1990 *Les alliages à mémoire de forme*. Paris: Hermès.
20. D. Brandon and R. C. Rogers 1992 *Journal of Intelligent Materials*, *Systems and Structures* **3**, 255. Constitutive laws for pseudo-elastic materials.
21. B. Raniecki, Ch. Lexcellent and K. Tanaka 1992 *Archiwum mechanikstosowanej* **44**, 261. Thermodynamic models of pseudoelastic behavior of shape memory alloys.
22. S. Y. Luo, F. Gordaninejad and C. D. Hong 1990 *Proceedings of the 5th Japan–US Conference on Composite Materials* **Tokyo**, 437. Constitutive relation of shape–memory flexible composites.
23. F. J. Lockett 1972 *Nonlinear Viscoelastic Solids*. London: Academic Press.
24. R. M. Christensen 1971 *Theory of Viscoelasticity*: *An introduction*. Academic Press Inc.
25. A. E. Green and R. S. Rivlin 1957 *Archive of Rationnal Mechanical Analysis* **1**, 1–21. The mechanics of non-linear materials with memory.